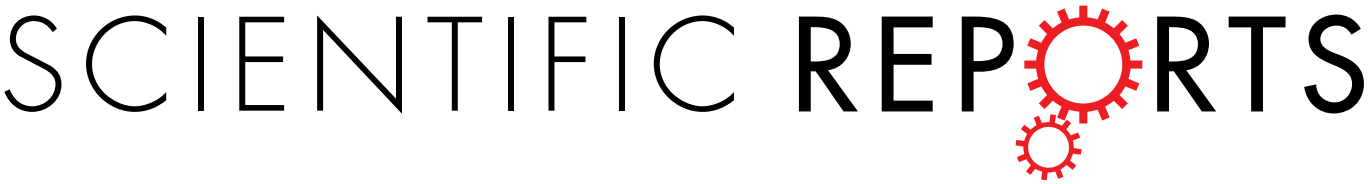

OPEN

Optical characterization of Tm^{3+} doped Bi_2O_3-GeO_2-Ga_2O_3 glasses in absence and presence of BaF_2

Received: 09 February 2016
Accepted: 14 July 2016
Published: 10 August 2016

Kexuan Han[1], Peng Zhang[1], Shunbin Wang[2], Yanyan Guo[1], Dechun Zhou[1] & Fengxia Yu[1]

In this paper, Two new Bi_2O_3-GeO_2-Ga_2O_3 glasses (one presence of BaF_2) doped with 1mol% Tm_2O_3 were prepared by melt-quenching technique. Differential thermal analysis (DTA), the absorption, Raman, IR spectra and fluorescence spectra were measured. The Judd–Ofelt intensity parameters, emission cross section, absorption cross section, and gain coefficient of Tm^{3+} ions were comparatively investigated. After the BaF_2 introduced, the glass showed a better thermal stability, lower phonon energy and weaker OH^- absorption coefficient, meanwhile, a larger ~1.8 μm emission cross section σ_{em} (7.56×10^{-21} cm^2) and a longer fluorescence lifetime τ_{mea} (2.25 ms) corresponding to the Tm^{3+}: $^4F_3 \rightarrow {}^3H_6$ transition were obtained, which is due to the addition of fluoride in glass could reduce the quenching rate of hydroxyls and raise the cross-relaxation ($^3H_6 + {}^3H_4 \rightarrow {}^3F_4 + {}^3F_4$) rate. Our results suggest that the Tm^{3+} doped Bi_2O_3-GeO_2-Ga_2O_3 glass with BaF_2 might be potential to the application in efficient ~1.8 μm lasers system.

Over the past decade, Tm^{3+}-doped fiber lasers have attracted growing attention in numerous areas owing to their very broad transition linewidth over ~1.7 to 2.1 μm wavelength[1–4]. As we know, near-infrared lasers at the eye-safe 2 μm region have many potential applications in medicine, remote sensing, and atmospheric pollutant monitoring[4,5]. Recently, the long-wavelength window around 1700 nm has attracted attention for OCT imaging[6]. Wavelengths near ~1720 nm are of interest for targeting fat/lipid-rich tissues due to the high absorption coefficient of human fat and low water scattering and absorption[7]. Nicholas G. Horton. *et al.* were put forward expectations that a wavelength-tunable source that covers the entire "low attenuation" spectral window from 1650 to 1850 nm can be obtained, which will further increase the number of accessible fluorophores and fluorescent proteins for Three-photon fluorescence microscopy (3PM) in the 1700 nm spectral window[8]. In addition, they can operate as pump sources for achieving 3.0~5.0 μm mid-infrared fiber lasers output at room-temperature, for national defense and commercial applications[9,10]. A typical work on Tm^{3+}-Tb^{3+} co-doped tunable fiber ring laser for 1716 nm lasing was pumped by a 1.21 μm laser diode[11]. Another type of Tm-doped silica fiber laser with narrow-linewidth and output wavelength near 1750 nm has been reported, by using a 1550 nm Er-doped fiber laser pump source and a volume Bragg grating (VBG)[12].

Tm^{3+} is a better solution to ~2 μm emissions because of its absorption band near 808 nm matching well with commercially available and high power laser diode[13]. Due to the cross-relaxation ($^3H_6 + {}^3H_4 \rightarrow {}^3F_4 + {}^3F_4$) process between Tm^{3+} ions, the ideal quantum efficiency of Tm^{3+}: $^3F_4$ can reach 200%[14,15]. To date, in order to get powerful infrared emissions from Tm^{3+} ions, various kinds of glass hosts have been investigated including silicate[16], tellurite[17], germanate[18], and fluorophosphates[19] glasses. Yin-Wen Lee, etc. reported an 18-dB 2013-nm amplifier which was demonstrated in a 50-cm 7 wt% Tm^{3+}-doped double-clad silicate fiber[20]. Xin Wen, etc. reported a multilongitudinal-mode fiber laser at 1.95 μm has also been achieved in a 10 cm long as-drawn active fiber, yielding a maximum laser output power of 165 mW and a slope efficiency of 17%[21]. Zhi-Xu Jia reported a supercontinuum generation in Tm^{3+} doped tellurite microstructured fibers pumped by a 1.56 μm femtosecond fiber laser[22]. However, few researches have been paid on the bismuth germanate glass and fiber.

Among the oxide glasses, the bismuthate glass has a lower phonon energy (~440 cm^{-1})[23,24] compared with silicate (~1000 cm^{-1})[16], germanate (~900 cm^{-1})[13] and tellurite (~750 cm^{-1})[17] glasses, which is very useful to enhance the luminescence quantum efficiency[23] of Tm^{3+} ions and reduce the multiphonon relaxation[24]. In addition, compared with silicate and other heavy metal oxide glasses, the bismuthate glass possesses many other material

[1]Changchun University of Science and Technology, 7089 Weixing Road, Changchun, Jilin, 130022, P. R. China. [2]Jilin University, Changchun, Jilin, 130012, P. R. China. Correspondence and requests for materials should be addressed to F.Y. (email: yufengxia2015@163.com)

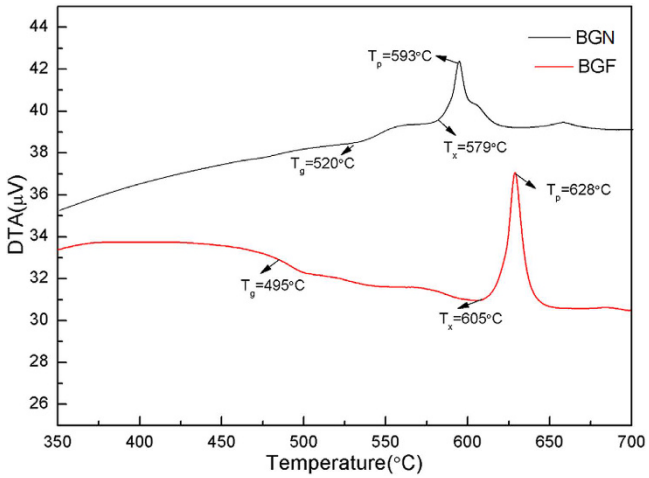

Figure 1. DTA curves of BGN and BGF glasses doped with 1 mol% Tm_2O_3 at the heating rate of 10 K/min.

advantages such as easy preparation process, low melting temperature, large rare-earth solubility[21], high refractive index (~2.1)[25] and wide transparency window[26], make bismuthate glass particularly promising for fiber amplifiers and infrared fiber lasers.

The OH^- groups may quench $^3F_4 \rightarrow {}^3H_6$ emissions of Tm^{3+} ions and reduce emission efficiency[5]. But hydroxyl and the fluorine ions are isoelectronic and their ionic size was similar; hydroxyl ions could easily be removed by fluoride during melting[27]. Therefore, 1 mol% Tm^{3+}-doped bismuth-germanium-gallate glasses in absence and presence of BaF_2 were studied for ~1.8 μm emission.

Experimental

Molar composition of $36Bi_2O_3- 29GeO_2- 25Ga_2O_3- 10Na_2O- 1Tm_2O_3$ (BGN) and $36Bi_2O_3- 29GeO_2- 25Ga_2O_3- 10BaF_2- 1Tm_2O_3$ (BGF) glasses were fabricated by conventional melting-quenching method in an alumina crucible at 1200 °C under oxygen atmosphere respectively. The glass samples were formed by casting molding and finally annealed at 480 °C for 3 h to remove thermal strains. Samples were cut and polished to $10 \times 10 \times 2$ mm^3 for property measurements.

Differential thermal analysis (DTA) was performed using a SETARAM TAG24 analyser, for characteristic temperatures (the temperature of glass transition T_g, temperature of onset crystallization T_x and temperature of peak crystallization T_p). Density and refractive index of samples was obtained by Archimedes method and spectroscopic ellipsometer method, respectively. The absorption spectrum was recorded using a spectrophotometer (Perkin Elmer Lambda9). The near-infrared emission spectra and luminescence lifetime were measured by FLSP920 (Edinburgh instruments Ltd., UK) under 808 nm laser diode pumped. Raman spectra were monitored with a FT Raman spectrophotometer (Nicolet Module). All measurements were carried out at room temperature.

Results and Discussions

Thermal property. Figure 1 shows the DTA curve of the studied glass, and the values of T_g, T_x and T_p in Tm^{3+}-doped BGN and BGF samples are indicated. The difference between the glass transition temperature T_g and the onset crystallization temperature T_x, $\Delta T = T_x - T_g$, has been frequently used as a rough estimate of glass formation ability or glass thermal stability. It can be seen that the values of T_g is decreased from 520 °C to 495 °C as the Na_2O is replaced by BaF_2 in BGF glass. However, it is still higher than of fluoride[28], tellurite[29] glasses, this results show that the glasses have good thermal shock resistance performance under the condition of high power pump. Generally, the ΔT of the glass sample should be higher than 100 °C to obtain a better thermal stability and to avoid crystallization during the optical fiber drawing process[30,31]. After the addition of BaF_2, the thermal stability (ΔT) of Bi_2O_3-GeO_2-Ga_2O_3 glass is increased quite significantly. The value of ΔT for BGF sample is 110 °C,which is higher than of BGN (59 °C), indicating that the BGF sample has better thermal stability against crystallization for ~1.8 μm emission.

Absorption and IR transmittance spectra. Figure 2 shows the absorption spectra of the Tm^{3+} doped BGN and BGF samples under room temperature. All absorption bands belong to transition of Tm^{3+} ions from ground state to higher levels are labeled in Fig. 2. As expected, BGN and BGF samples have similar absorption peaks, and the $^3H_6$-$^1G_4$ transition has not appeared, due to the UV cut-off wavelength of bismuthate glasses is redshift. Strong absorption around 790 nm indicates that these glasses can be excited efficiently by 808 nm LD. As shown in Fig. 3, BGF sample shows better IR transmittance than BGN sample. The absorption band ranging from 2700 to 3700 cm^{-1} is due to stretching vibrations of free OH^- groups. Hydroxyl and the fluorine ions are isoelectronic and their ionic size is similar[28], hydroxyl ions can easily be removed by fluoride during melting through the reaction $OH^- + F^- \rightarrow HF + O^{2-}$. The OH^- absorption coefficient in the glass can be calculated by the IR transmission spectra, which is given by[31]

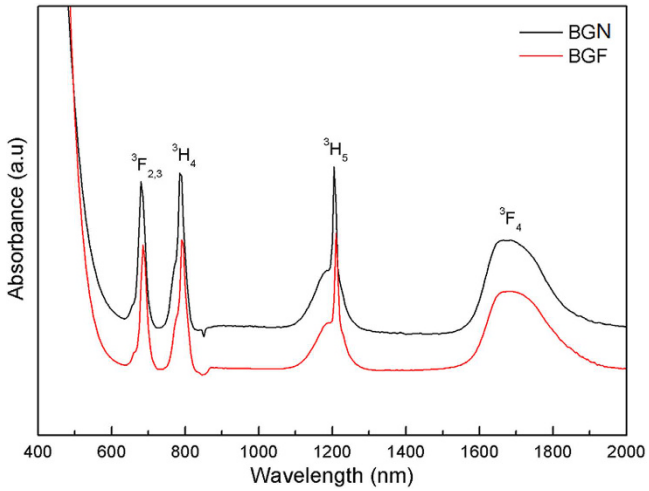

Figure 2. Room temperature absorption spectra in the range from 400 to 2000 nm of the BGN and BGF glass samples doped with 1 mol% of Tm_2O_3.

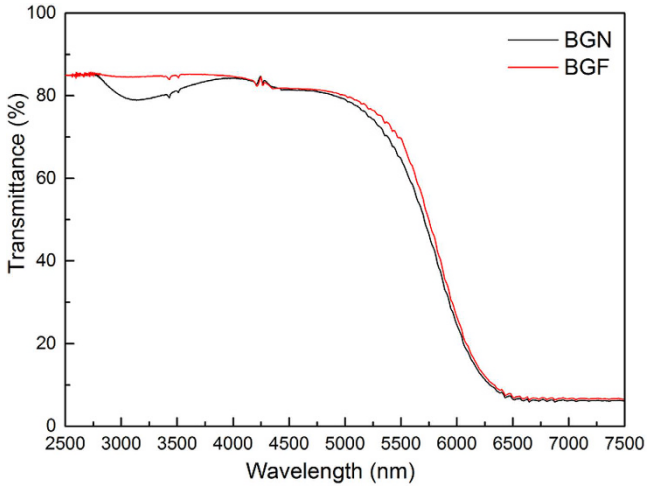

Figure 3. Infrared transmission spectrum of the BGN and BGF glasses doped with 1 mol% of Tm_2O_3 in the range of the absorption bands of water.

$$\alpha_{OH} = 2.303 \ \log \frac{T_0}{T}/l \tag{1}$$

where l is the thickness of a sample, T_0 and T are the transmission value of maximum and at 3000 cm^{-1}, respectively. The OH^- absorption coefficient of BGN and BGF samples are calculated according to Eq. (1), 0.34 cm^{-1} and 0.05 cm^{-1}, respectively. It is obvious that typical OH^- groups' absorption of BGN sample is much stronger than that of BGF sample at 3 μm regions, which is one of the main reasons for the difference between BGN and BGF samples in ~1.8 μm emission.

Judd-Ofelt analysis. According to absorption spectra (Fig. 1), Judd-Ofelt (J-O) theory has been applied to determine the important spectroscopic and laser parameters of Tm^{3+} ion. In this paper, J-O intensity parameters Ω_t ($t = 2$, 4, and 6) are calculated and radiative transitions within $4f^n$ configuration of Tm^{3+} is analyzed, the value of them list in Table 1. The value Ω_2 of BGF are lower than those of BGN, however, they are still much larger than that of silicate[31], tellurite[32], fluoride[33] and germanate[34] glasses. As known Ω_2 is related with the covalency between rare earth ions and ligands anions and reflects the asymmetry of local environment at Tm^{3+} site in the glass hosts. Large Ω_2 means stronger covalency between the rare-earth ions and ligand anions, while the Ω_6 has a relation with the overlap integrals of $4f$ and $5d$ orbits[26]. Large value of Ω_6 exhibits the large value of emission bandwidth and spontaneous radiative probability of rare earth[31]. Values of Ω_4 and Ω_6 also provide some information on the rigidity and viscosity of hosts.

Glass	Ω_2 ($\times 10^{-20}$ cm^2)	Ω_4 ($\times 10^{-20}$ cm^2)	Ω_6 ($\times 10^{-20}$ cm^2)	Reference
BGN	6.26	0.24	1.6	This work
BGF	5.15	1.01	1.25	
silicate	3.40	0.46	0.66	16
Tellurite	3.20	2.01	1.83	29
Fluorophosphate	3.01	2.56	1.54	32
Germanate	3.93	1.1	1.1	35

Table 1. Judd-Ofelt intensity parameters in BGN and BGF samples.

			BGN sample				BGF sample		
Transition	λ (nm)	A_{rad} (s^{-1})	∑A (s^{-1})	β (%)	τ (ms)	A_{rad} (s^{-1})	∑A (s^{-1})	β (%)	τ (ms)
$^3F_4 \rightarrow {}^3H_6$	1847	454.48	454.48	100	2.20	406.38	406.38	100.00	2.46
$^3H_5 \rightarrow {}^3F_4$	3563	27.5	609.08	4.53	1.64	21.45	507.51	4.23	1.97
$\rightarrow {}^3H_6$	1216	581.51		95.47		486.07		95.77	
$^3H_4 \rightarrow {}^3H_5$	2428	10.81	3679.83	0.29	0.27	26.49	2894.29	0.92	0.35
$\rightarrow {}^3F_4$	1444	283.61		7.71		235.88		8.15	
$\rightarrow {}^3H_6$	810	3385.40		92.00		2631.92		90.93	
$^3F_3 \rightarrow {}^3H_4$	5200	7.05	4938.24	0.14	0.20	7.00	4302.28	0.16	0.23
$\rightarrow {}^3H_5$	1655	832.61		16.86		685.69		15.94	
$\rightarrow {}^3F_4$	1310	184.22		3.73		133.42		3.10	
$\rightarrow {}^3H_6$	701	3914.36		79.27		3476.17		80.80	
$^3F_2 \rightarrow {}^3F_3$	20449	0.01	2155.96	0.00	0.46	0.01	1639.24	0.00	0.61
$\rightarrow {}^3H_4$	4145	41.78		1.94		33.83		2.06	
$\rightarrow {}^3H_5$	1531	370.17		17.17		347.88		21.22	
$\rightarrow {}^3F_4$	10722	2.09		0.10		1.63		0.10	
$\rightarrow {}^3H_6$	678	1741.92		80.80		1255.88		76.61	
$^1G_4 \rightarrow {}^3F_2$	1632	20.61	5445.72	0.38	0.18	24.28	4493.39	0.54	0.22
$\rightarrow {}^3F_3$	1511	118.63		2.18		97.46		2.17	
$\rightarrow {}^3H_4$	1171	714.61		13.12		533.45		11.87	
$\rightarrow {}^3H_5$	790	1946.18		35.74		1434.64		31.93	
$\rightarrow {}^3F_4$	647	383.41		7.04		318.74		7.09	
$\rightarrow {}^3H_6$	479	2262.29		41.54		2084.82		46.40	
$^1D_2 \rightarrow {}^1G_4$	1538	432.58	71946.23	0.60	0.01	374.52	62466.60	0.60	0.02
$\rightarrow {}^3F_2$	792	1258.84		1.75		1569.68		2.51	
$\rightarrow {}^3F_3$	762	3113.90		4.33		2523.72		4.04	
$\rightarrow {}^3H_4$	665	5208.87		7.24		3930.55		6.29	
$\rightarrow {}^3H_5$	522	244.90		0.34		188.45		0.30	
$\rightarrow {}^3F_4$	455	55623.17		77.31		43031.91		68.89	
$\rightarrow {}^3H_6$	365	6063.96		8.43		10847.76		17.37	
$^1I_6 \rightarrow {}^1D_2$	1424	0.00	25009.80	0.00	0.04	0.00	26885.62	0.00	0.04
$\rightarrow {}^1G_4$	739	3182.74		12.73		3497.78		13.01	
$\rightarrow {}^3F_2$	509	2202.92		8.81		1707.47		6.35	
$\rightarrow {}^3F_3$	497	55.70		0.22		49.53		0.18	
$\rightarrow {}^3H_4$	453	3851.15		15.40		4264.61		15.86	
$\rightarrow {}^3H_5$	382	150.15		0.60		125.55		0.47	
$\rightarrow {}^3F_4$	345	14686.53		58.72		15939.71		59.29	
$\rightarrow {}^3H_6$	291	880.60		3.52		1300.96		4.84	

Table 2. Calculated radiative properties in BGN and BGF samples. $\sum A$ is the total spontaneous emission probability of each level, A_{rad} is the spontaneous emission probability of each transition, τ is the calculated radiative lifetime.

As shown in Table 2, spontaneous emission probability (A) for Tm^{3+} can also be calculated by using J-O theory, which is related with the J-O parameters and the refractive-index of host glass. Total spontaneous emission probability ($\sum A$) of Tm^{3+}: $^3F_4$ level in BGN glass (454.8 s^{-1}) is higher than that in BGF glass (406.38 s^{-1}), so is the A_{rad} of transition Tm^{3+}: $^3H_4 \rightarrow {}^3F_4$. High A value in BGN suggests strong emission, especially the ~1.8 μm emission. Lower A and Higher τ in BGF are owing to the addition of fluoride could reduce the refractive-index and

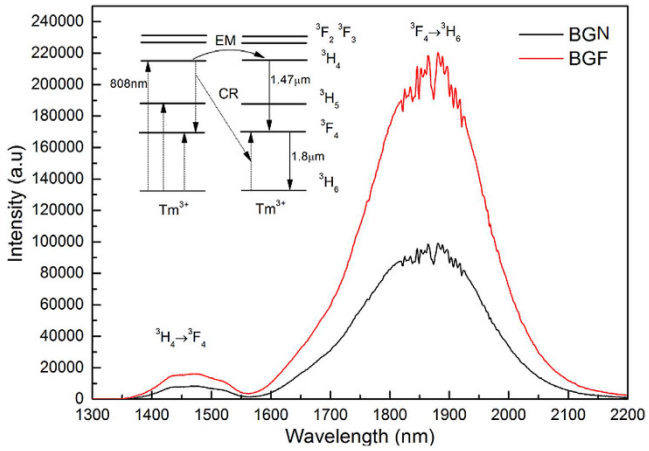

Figure 4. Room temperature ~1.8 μm emission spectra obtained by exciting with a cw laser diode at 808 nm for the BGN and BGF glasses doped with 1 mol% of Tm_2O_3. The inset is the energy level diagram and energy transfer sketch map of Tm^{3+} when pumped at 808 nm.

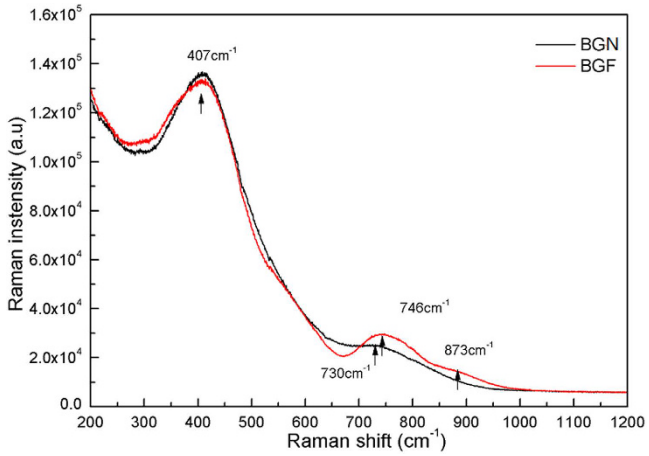

Figure 5. Raman spectra of BGN and BGF host glass samples in the range from 200 to 1200 cm^{-1}.

J-O parameters in bismuthate glass system. Compared with calculated radiative properties in germanate glasses[35], BGN and BGF samples have higher A_{rad} value for each transition.

Emission properties. Figure 4 shows the ~1.47 μm and ~1.8 μm emission spectra in BGN and BGF samples under 808 LD pumped. After the BaF_2 introduced, peak intensity of the ~1.8 μm emission in BGF is 2 times higher than that in BGN, while the intensity of ~1.47 emission is only a little change between two samples. As shown in the insert Fig. 4, the large intensity ratio of ~1800 nm to ~1470 nm (I_{1800}/I_{1470}) is related to the cross-relaxation (CR, $^3H_6 + {}^3H_4 \rightarrow {}^3F_4 + {}^3F_4$)[36].

With the introduction of BaF_2, the maximum phonon energy of glass hosts lower accordingly, which can be seen from the measured Raman spectra shown in Fig. 5, the maximum phonon energy of BGN and BGF samples can be presumed about 746 cm^{-1} and 730 cm^{-1}, respectively. The Raman scattering band higher than 700 cm^{-1} is mainly caused by the vibration of the tetrahedron group, the peak bond located in 756 cm^{-1} and 846 cm^{-1}, correspond to the structure unit vibration of Ge-O and Ga-O, respectively[34]. For BGF sample, lower phonon energy is also a key factor for stronger ~1.8 μm emissions.

According to the Fuchtbauer-Ladenburg theory, ~1.8 μm emission cross section (σ_{em}) is calculated[5].

$$\sigma_{em} = \frac{\lambda^4 A_{rad}}{8\pi c n^2} \frac{\lambda I(\lambda)}{\int \lambda I(\lambda) d\lambda} \tag{2}$$

where λ is the wavelength, A_{rad} is the spontaneous emission probability calculated by J-O theory, $I(\lambda)$ is the fluorescence intensity, n is the refractive index of the glass, and c is the light speed. It is noted that σ_{em} mainly related to ~1.8 μm emission spectrum and radiative transition probability of Tm^{3+}: $^3F_4 \rightarrow {}^3H_6$, which is a normalized line-shape function, respectively. According to Eq. (3), the stimulated emission cross-sections (σ_{em}) of ~1800 nm calculated are shown in Fig. 6. It can be determined that σ_{em} of BGF sample performs a maximum 7.56×10^{-21} cm^2 at 1865 nm, which is higher than that of BGN sample (7.01×10^{-21} cm^2, centered at 1865 nm).

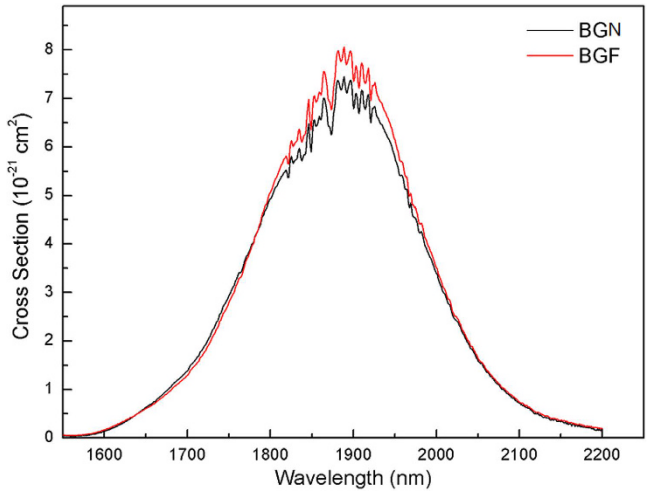

Figure 6. Stimulated emission cross-section of Tm^{3+}:$^3F_4 \rightarrow {}^3H_6$ transition in BGN and BGF glasses doped with 1 mol% Tm_2O_3.

Glass	σ_{em} ($\times 10^{-21}$ cm^2)	τ_{rad} (ms)	$\sigma_{em} \times \tau_{rad}$ ($\times 10^{-21}$ cm^2 ms)	Reference
BGN	7.01	2.25	15.42	This work
BGF	7.56	2.46	18.59	
silicate	3.6	7.91	28.48	28
Tellurite	8.1	1.73	14.00	24
Germanate	7.7	1.77	13.60	37

Table 3. Calculated emission cross-sections σ_{em}, radiative lifetime τ_{rad}, and $\sigma_{em} \times \tau_{rad}$ of Tm^{3+}: $^3F_4 \rightarrow {}^3H_6$ in BGN and BGF samples.

For BGN and BGF samples, the values of the maximum stimulated emission cross-section at the wavelength of 1865 nm, which are larger than that of the fluorophosphate glasses[37], silicate glasses[2,16,31] and germanate glasses[38], due to high refractive index, high J-O parameters and good emission, and are beneficial to ~1.8 μm laser action of Tm^{3+} ions.

The product of emission cross-section and radiative lifetime $\sigma_{em} \times \tau_{rad}$ is an important parameter for laser materials to obtain high gain. As shown in Table 3, the calculated values $\sigma_{em} \times \tau_{rad}$ of BGN and BGF samples are 15.42×10^{-21} cm^2 ms and 18.59×10^{-21} cm^2 ms, respectively, which are lower than silicate glass[31] $\sigma_{em} \times \tau_{rad} = 28.48 \times 10^{-21}$ cm^2 ms. However, There are still larger than tellurite glass[24] $\sigma_{em} \times \tau_{rad} = 14.00 \times 10^{-21}$ cm^2 ms and germanate glasses[38] $\sigma_{em} \times \tau_{rad} = 13.6 \times 10^{-21}$ cm^2 ms.

Cross-relaxation process. Because of the cross-relaxation transfer process ($^3H_6 + {}^3H_4 \rightarrow {}^3F_4 + {}^3F_4$) is beneficial for the ~1800 nm emission[5]. It is necessary to study the cross-relaxation process between Tm^{3+} ions. According to the theory of Dexter and Forster, the cross-relaxation rate can be calculated by the integral overlap of absorption cross-sections and emission cross-sections[33], which belongs to a dipole–dipole interaction. The microscopic transfer probability can be expressed by[34]

$$W_{D-A} = \frac{C_{D-A}}{R^6} \tag{3}$$

where R is the distance between donor and acceptor, C_{D-A} is the transfer constant defined as follows[15] $C_{D-A} = R_c^6/\tau_D$, where R_c is the critical radius of the interaction and τ_D is the intrinsic lifetime of the donor-excited level. The transfer constant can be obtained according to Eq. (4) when phonons participate in the process to balance the energy gap[5].

$$C_{D-A} = \frac{6cg_{low}^D}{(2\pi)^4 n^2 g_{low}^D} \sum_0^\infty e^{-(2\bar{n}+1)S_0} \frac{S_0^m}{m!} (\bar{n}+1)^m \int \sigma_{emis}^D(\lambda_m^+) \sigma_{abs}^A(\lambda) d\lambda \tag{4}$$

where c is the light speed, n is the refractive index, g_{low}^D/g_{up}^D is the degeneracy of the lower and upper levels of the donor, respectively, $\bar{n} = (1/e^{\hbar w_0/KT} - 1)$ is the average occupancy of the phonon mode at temperature T, $\hbar\omega_0$ is the maximum phonon energy, m is the number of phonons that participate in the energy transfer, S_0 is Huang–Rhys factor (0.31 for Tm^{3+})[5], and $\lambda_m^+ = (1/\lambda - m\hbar\omega_0)$ is the wavelength with m phonon creation. The caculated energy migration (EM, $^3H_4 + {}^3H_6 \rightarrow {}^3H_6 + {}^3H_4$) and cross relaxation (CR, $^3H_6 + {}^3H_4 \rightarrow {}^3F_4 + {}^3F_4$) processes in BG

Glass	EM		CR		
	M% phonons	C_{D-D} (10^{-40} cm^6/s)	M% phonons	C_{D-A} (10^{-40} cm^6/s)	W_{ET} (10^{-20} cm^3/s)
BGN	0, 1	35.4	0, 1, 2	16.0	938
	99.99, 0.01		12.78, 83.99, 3.23		
BGF	0, 1	37.8	0, 1, 2	18.6	1020
	99.99, 0.01		16.07, 79.37, 4.56		

Table 4. Energy transfer parameters of the energy migration and cross-relaxation processes in BGN and BGF samples.

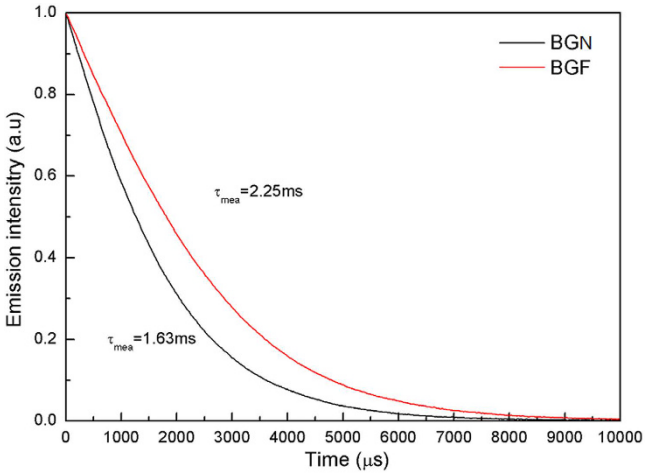

Figure 7. Luminescence decay curves of the $^3F_4$ level of the Tm^{3+} ions obtained exciting resonantly the $^3H_6 \rightarrow {}^3H_4$ absorption transition at 808 nm and monitoring the Tm^{3+} $^3F_4 \rightarrow {}^3H_6$ emission at 1865 nm in BGN and BGF glasses doped with 1 mol% Tm_2O_3.

and BGF are listed in Table 4. Because of the transfer condition of C_{D-D} is much larger than C_{D-A}, the hopping model is fulfilled in both BGN and BGF. to evaluate the energy transfer rate W_{ET}[39],

$$W_{ET} = 13(C_{D-D})^{1/2}/(C_{D-A})^{1/2} n_D \tag{5}$$

where n_D is the concentration of donor. According to Eq. (5), W_{ET} is calculated to be 938 cm^3/s and 1020 cm^3/s in BGN and BGF, respectively.

Fluorescence lifetime. The fluorescence decays of the Tm^{3+}: $^3F_4$ level at room temperature is shown in Fig. 7. It can be seen that the measured lifetime τ_{mea} in BGN and BGF are 1.63 ms and 2.25 ms, respectively. The quantum efficiency (η) of the $^3F_4 \rightarrow {}^3H_6$ emission can be calculated by

$$\eta = \frac{\tau_{mea}}{\tau_{rad}} \tag{6}$$

where τ_{mea} is the measured fluorescence lifetime and τ_{rad} is calculated with the Judd–Ofelt formalism. According to Eq. (6), the values of quantum efficiency for BGN and BGF are 74.09% and 91.46%, respectively, which are higher than silicate glass (13%)[31], germanate glasss (55.52%)[5], and lower than $70TeO_2$-$20ZnO$-$10ZnF_2$ glass (164%)[40]. The larger radiative lifetime (τ_{mea}) of Tm^{3+}: $^3F_4$ state is benefit for ~1.8 μm laser action. It can be seen that the measured lifetime is shorter than the calculated lifetime, due to nonradiative quenching[31]. The nonradiative decay caused from several mechanisms, such as energy transfer between the Tm^{3+} ions, multiphonon decay[29], quenching by impurities (OH^-), etc. The total rate of the $^3F_4 \rightarrow {}^3H_6$ transition can be evaluated by[41,42]:

$$\frac{1}{\tau_{mea}} = \frac{1}{\tau_{cal}} + W_{NR} = \frac{1}{\tau_{cal}} + W_{MPR} + W_{OH^{-1}} + W_{ET} \tag{7}$$

where $1/\tau_{cal}$ is the spontaneous radiative probability A_{rad}, W_{MPR} is the nonradiative multiphonon relaxation rate, $W_{OH}{}^{-1}$ is the nonradiative transition probability due to the energy transfer to OH^- impurities and W_{ET} represents an additional nonradiative loss mechanism due to the energy transfer between the RE ions. In this study, the concentrations of Tm^{3+} ions for BGN and BGF are the same, this third process can be neglected.

The multiphonon relaxation W_{MPR} can be expressed[43]:

$$W_{MPR} = W_0 \exp\left(-\frac{1}{\hbar\omega_{max}}\left(\ln\frac{p}{g-1}\right)\Delta E\right) \quad (8)$$

where W_0 is an experimentally determined parameter which is independent of the particular RE ion. ΔE is the energy gap between the $^3F_4$ and $^3H_6$ levels. g is the electron-phonon coupling strength parameter, and $\hbar\omega_{max}$ is the highest phonon energy obtained from Raman spectra and $p = \Delta E/\hbar\omega_{max}$. Multiphonon decay depends on the number of phonons required to bridge the energy gap to the next lower lying manifold. The higher the $\hbar\omega_{max}$ is, the larger the multiphonon relaxation is.

W_{OH^-} is proportional to the concentration of Tm^{3+} ions and the measured absorption coefficient of OH^- groups[42,44]. For BGF sample, after BaF_2 introduced, the α_{OH^-} shows a significantly decrease, $W_{OH^-}{}^{-1}$ is expected to decrease which results in a reduced nonradiative transition rate. Thus the lifetime is much longer while the quantum efficiency is higher in BGF. Generally, the relatively longer radiation lifetime is beneficial to reduce the laser oscillation threshold[45].

Conclusion

In conclusion, we reported on ~1.8 μm emission in Tm^{3+}-doped Bi_2O_3-GeO_2-Ga_2O_3 glasses in absence and presence of BaF_2. The addition of BaF_2 not only influences the network of glass, but also effectively reduces the content of hydroxyls and maximum phonon energy. For BGF sample, it shows a better thermal stability, and a stronger ~1.8 μm emission than that in BGN sample. It is also found that BGF glass possesses relatively large ~1.8 μm emission cross-section σ_{em} (7.56×10^{-21} cm^2), measured fluorescence lifetime τ_{mea} (2.25 ms) and figure of merit gain $\sigma_{em} \times \tau_{rad}$ (14.69×10^{-21} cm^2 ms) corresponding to the Tm^{3+}: $^3F_4 \rightarrow {}^3H_6$ transition. Our results suggest that introduced the BaF_2 into the glass network structure, which paves a way to enhance the ~1.8 μm emission properties and improve the fluorescence lifetime of Tm^{3+}: $^3F_4$ in Tm^{3+} doped bismuthate glass.

References

1. Balda, R. *et al.* Spectroscopic properties of the 1.4 μm emission of Tm^{3+} ions in TeO_2-WO_3-PbO glasses. *Opt.Express*. **16,** 11836–11846 (2008).
2. Allain, J. Y. Monerie, M. & Poignant, H. Tunable cw lasing around 0.82, 1.48, 1.88, and 2.35 μm in thulium doped fluorozirconate fiber. *Electron. Lett*. **25,** 1660–1662 (1989).
3. Tanabe, S. Feng, X. & Hanada, T. Improved emission of Tm^{3+}-doped glass for a 1.4 μm amplifier by radiative energy transfer between Tm^{3+} and Nd^{3+}. *Opt. Lett*. **25,** 817–819 (2000).
4. Wu, J. Yao, Z. Zong, J. & Jiang, S. Highly efficient high-power thulium-doped germanate glass fiber laser. *Opt. Lett*. **32,** 638–640 (2007).
5. Gao, S. *et al.* 2 μm emission properties and non-radiative processes of Tm^{3+} in germanate glass. *J. Appl. Phys.* **116,** 173108-1-6 (2014).
6. Shutaro, I. & Norihiko, N. Quantitative comparison of contrast and imaging depth of ultrahigh-resolution optical coherence tomography images in 800–1700 nm wavelength region. *Biomed. Opt. Express*. **3,** 282–294 (2012).
7. Alexander, V. V. *et al.* Photothermolysis of Sebaceous Glands in Human Skin *Ex Vivo* with a 1,708 nm Raman Fiber Laser and Contact Cooling. *Lasers Surg Med*. **43,** 470–480 (2011).
8. Horton, N. G. *et al. In vivo* three-photon microscopy of subcortical structures within an intact mouse brain. *Nature Photon*. **7,** 205–209 (2013).
9. Willer, U. *et al.* Near- and mid-infrared laser monitoring of industrial processer, environment and security applications. *Opt. Laser Eng*. **44,** 699–710 (2006).
10. Jackson, S. & Towars, D. high-power mid-infrared emission from a fiber laser. *Nature. Photo*. **6,** 423–431 (2012).
11. Yamada, M. *et al.* Tm^{3+}-Tb^{3+}-doped tunable fibre ring laser for 1700 nm wavelength region. *Electron. Lett.* **49,** 1287–1288 (2013).
12. Zhao, Q. *et al.* 400 mW narrow-linewidth Tm-doped silica fiber laser output near 1750 nm with volume Bragg grating. *Sci. Rep.* **5,** 12034 (2015).
13. Yuan. J. *et al.* Efficient 2.0 μm emission in Nd^{3+}/Ho^{3+} co-doped tungsten tellurite glasses for a diode-pump 2.0 μm laser. *J. Appl. Phys.* **113,** 173507-1-5 (2013).
14. Turri, G. *et al.* Temperature-dependent spectroscopic properties of Tm^{3+} in germanate, silica, and phosphate glasses: A comparative study. *J. Appl. Phys*. **103,** 093104–093107 (2008).
15. Shin, Y. B. Cho, W. Y. & Heo, J. Multiphonon and cross relaxation phenomena in Ge-As (or Ga) -S glasses doped with Tm^{3+}. *J. Non-Crystal. Solids* **208,** 29–35 (1996).
16. Liu, X. *et al.* ~2 μm Luminescence properties and nonradiative processes of Tm^{3+} in silicate glass. *J. Lumin.* **150,** 40–45 (2014).
17. Zhou, Y. *et al.* Enhanced 2 μm fluorescence and thermal stability in Ho^{3+}/Tm^{3+}codoped WO_3 modified tellurite glasses. *Mater. Lett*. **142,** 277–279 (2015).
18. Wang, W. C. *et al.* An efficient 1.8 μm emission in Tm^{3+} and Yb^{3+}/Tm^{3+} doped fluoride modified germanate glasses for a diode-pump mid-infrared laser. *J. Non-Cryst.Solids*. **404,** 19–25 (2014).
19. Wang, M. *et al.* Enhanced 2 μm emission of Yb–Ho doped fluorophosphates glass. *J. Non-Cryst.Solids* **357,** 2447–2449 (2011).
20. Lee, Y. W. *et al.* Heavily Tm^{3+}-Doped Silicate Fiber for High-Gain Fiber Amplifiers. *Fibers*. **1,** 82–92 (2013).
21. Wen, X. *et al.* Highly Tm3+ doped germanate glass and its single mode fiber for 2.0 μm laser. *Sci. Rep.* **6,** 20344 (2016).
22. Jia, Z. X. *et al.* Supercontinuum generation and lasing in thulium doped tellurite microstructured fibers. *J. Appl. Phys.* **115,** 063106 (2014).
23. Sontakke, A. D. & Annapurna, K. Spectroscopic properties and concentration effects on luminescence behavior of Nd^{3+} doped Zinc–Boro–Bismuthate glasses. *Mater. Chem. Phys.* **137,** 916–921 (2013).
24. Li, K. *et al.* Broadband near-infrared emission in Er^{3+}-Tm^{3+} co-doped bismuthate glasses. *J. Alloys Compd.* **509,** 3070–3073 (2011).
25. Fan, H. *et al.* Tm^{3+} doped Bi_2O_3–GeO_2–Na_2O glasses for 1.8 μm fluorescence. *Opt. Mater.* **32,** 627–631 (2010).
26. Guo, Y. Li, M. Hu, L. & Zhang, J. Intense 2.7 μm emission and structural origin in Er^{3+}-doped bismuthate (Bi_2O_3-GeO_2-Ga_2O_3-Na_2O) glass. *Opt. Lett.* **37,** 268–270 (2012).
27. Lachheb, R. *et al.* Characterization of Tm^{3+} doped TNZL glass laser material. *J. Lumin.* **161,** 281–287 (2015).
28. Wang, G. *et al.* Effect of F^- ions on emission cross-section and fluorescence lifetime of Yb^{3+}-doped tellurite glasses. *J. Non-Crystal. Solids* **351,** 2147–2151 (2005).
29. Manikandan, N. Ryasnyanskiy, A. & Toulouse, J. Thermal and optical properties of TeO_2–ZnO–BaO glasses. *J. Non-Cryst. Solids* **358,** 947–951 (2012).
30. Gao, S. *et al.* Mechanical and ~2 μm emission properties of Tm^{3+}-doped GeO_2-TeO_2 (or SiO_2)-PbO-CaO glasses. *Opt. Mater.* **45,** 167–170 (2015).

31. Li, M. *et al.* Investigation on Tm^{3+}-doped silicate glass for 1.8 μm emission. *J. Lumin.* **132,** 1830–1835 (2012).
32. Tanabe, S. *et al.* Relation between the Ω_6 intensity parameter of Er^{3+} ions and the ^{151}Eu isomer shift in oxide glasses. *J. Appl. Phys.* **73,** 8451–8454 (1993).
33. Guo, H. *et al.* Host dependence of spectroscopic properties of Dy^{3+}-doped and Dy^{3+}. Tm^{3+}-codped Ge-Ga-S-CdI_2 chalcohalide glasses. *Opt.Express*. **17,** 15350–15350 (2009).
34. Moulton, P. F. *et al.* Tm-Doped Fiber Lasers: Fundamentals and Power Scaling. *Selected Topics in Quantum Electronics. IEEE Journal of.* **15,** 85–92 (2009).
35. Peng, Y. *et al.* The effect of La_2O_3 in Tm^{3+}-doped germanate-tellurite glasses for ~2 μm emission. *Sci. Rep*. **4,** 5256 (2014).
36. Dexter, D. L. A theory of sensitized luminescence in solids. *J. Chem. Phys*. **21,** 836–850 (1953).
37. Tian, Y. *et al.* 1.8 μm emission of highly thulium doped fluorophosphate glasses. *J. Appl. Phys*. **108,** 083504-1-7 (2010).
38. Balda, R. *et al.* Optical spectroscopy of Tm^{3+} ions in GeO_2–PbO–Nb_2O_5 glasses. *Opt. Mater*. **27,** 1771–1775 (2005).
39. Sousa, D. & de Nunes, L. Microscopic and macroscopic parameters of energy transfer between Tm^{3+} ions in fluoroindogallate glasses. *Phys. Rev. B* **66,** 024207-1-6 (2002).
40. Xu, R., Tian, Y., Hu, L. & Zhang, J. 2 μm spectroscopic investigation of Tm^{3+}-doped tellurite glass fiber. *J. Non-Crystal. Solids* **357,** 2489–2493 (2011).
41. Yaoyao, Ma. *et al.* Increased radiative lifetime of Tm^{3+}: $^3F_4 \rightarrow {}^3H_6$ transition in oxyfluoride tellurite glasses. *Mater. Res. Bull*. **64,** 262–266 (2015).
42. Layne, C. B. Lowdermilk, W. H. & Weber, M. J. Multiphonon relaxation of rare-earth ions in oxide glasses, *Phys. Rev. B* **16,** 10–20 (1977).
43. Miyakawa, T. & Dexter, D. L. Phonon Sidebands, Multiphonon relaxation of excited states, and phonon-assisted energy transfer between ions in solids. *Phys. Rev. B* **1,** 2961–2696 (1970).
44. Jacinto, C. *et al.* Thermal lens study of the OH^- influence on the fluorescence efficiency of Yb^{3+}-doped phosphate glasses. *Appl. Phys. Lett*. **86,** 071911–071913 (2005).
45. Zhang, Q. *et al.* Spectroscopic properties of Ho^{3+}/Yb^{3+} codoped lanthanum aluminum germanate glasses with efficient energy transfer. *J. Appl. Phys*. **106,** 113102-113102-5 (2009).

Acknowledgements

This work is financially supported by National Natural Science Foundation of China (No. 51502022).

Author Contributions

K.H., P.Z. and Y.G. and designed the experiments wrote the main manuscript text, F.Y. and D.Z. checked up. S.W. performed the experimental measurement. All authors reviewed the manuscript.

Additional Information

Competing financial interests: The authors declare no competing financial interests.

How to cite this article: Han, K. *et al.* Optical characterization of Tm^{3+} doped Bi_2O_3-GeO_2-Ga_2O_3 glasses in absence and presence of BaF_2. *Sci. Rep.* **6**, 31207; doi: 10.1038/srep31207 (2016).